Reaction-Condition-Dependent Active-Site Formation in Mixed-Oxide Catalysts for Syngas Conversion

Authors

Wei Ming Tan[1*], Jia Hui Lim[2], Daniel Kai Chen[3]

Affiliations

Department of Chemical and Biomolecular Engineering, College of Design and Engineering, National University of Singapore, 4 Engineering Drive 4, Singapore 117585

***Corresponding author:** WMingTan@nus.edu.sg

Abstract

The active sites of mixed-oxide catalysts often form dynamically under reaction conditions, making their identification difficult by ex situ characterization alone. Herein, first-principles thermodynamics and density functional theory were combined to identify active-site motifs in Zn–Cr–O catalysts for syngas conversion. More than 96 surface models were constructed by varying Zn/Cr ratios, oxygen chemical potential, hydroxyl coverage, and surface vacancy concentration. The results show that partially reduced Zn–O–Cr ensembles are thermodynamically favored under H_2-rich conditions and provide lower barriers for CO activation and C–O bond hydrogenation. The calculated barrier for CH_3O* formation decreased from 1.21 eV on stoichiometric Cr_2O_3 to 0.82 eV on Zn-enriched mixed-oxide surfaces. Microkinetic simulations predicted a 2.9-fold increase in oxygenate formation rate when reduced Zn–O–Cr motifs accounted for more than 35% of surface sites. These findings highlight the importance of reaction-induced active-site generation in oxide catalysis.

Keywords: first-principles calculation; mixed oxide; active site; syngas conversion; Zn–Cr catalyst; surface thermodynamics

1. Introduction

Syngas conversion provides an important route for transforming carbon-containing feedstocks into methanol, higher alcohols, light olefins, aromatics, and liquid fuels. Among the catalytic systems developed for this purpose, oxide–zeolite bifunctional catalysts have attracted considerable attention because they divide the overall reaction into two coupled functions. The oxide component activates CO and H_2 and generates oxygenated intermediates, whereas the zeolite component converts these intermediates through C–C coupling, cracking, oligomerization, cyclization, and aromatization. This separation of functions provides greater flexibility in controlling product distribution than conventional Fischer–Tropsch catalysts. Zn-based mixed oxides are particularly attractive because their metal composition, oxygen-vacancy concentration, redox properties, and local coordination environment can be adjusted over a relatively wide range. Studies of $ZnCrO_x$, $ZnGaO_x$, and $ZnZrO_x$ have demonstrated that the nature and formation rate of

oxygenated intermediates on the oxide strongly influence the subsequent hydrocarbon distribution over the zeolite [1,2]. More broadly, recent mechanistic studies of oxide–metal catalytic interfaces have shown that catalytic performance cannot always be described by a single ideal active-site geometry. Calculations based on ensembles of structurally distinct interfacial sites revealed pronounced differences in reaction mechanism, intrinsic reactivity, and deactivation behavior among local catalytic configurations [3]. This finding highlights the importance of describing working catalysts as populations of reaction-dependent surface structures rather than as a single static structural model.

Zn–Cr mixed oxides are especially relevant to high-temperature syngas conversion because of their thermal stability, tunable redox chemistry, and ability to activate both CO and H_2. When coupled with SAPO-34, H-SSZ-13, MCM-49, or ZSM-5, Zn–Cr oxides have been used to produce light olefins, aromatics, and gasoline-range hydrocarbons with product distributions that differ substantially from those obtained over the oxide alone [4,5]. The catalytic behavior of these systems is sensitive to the Zn/Cr ratio, crystallite size, preparation method, degree of reduction, oxygen-vacancy concentration, oxide–zeolite proximity, and zeolite acidity. These parameters affect not only the number of oxygenate-forming sites but also the type and lifetime of intermediates transferred to the zeolite [6,7]. Methanol, dimethyl ether, ketene, and other C_1 or C_2 oxygenates have all been proposed as possible intermediates in oxide–zeolite syngas conversion, and their relative importance can vary with catalyst composition and reaction conditions. Consequently, the identity of the oxide active site is directly connected to hydrocarbon selectivity. Despite extensive experimental and theoretical work, however, the local structure of the catalytically relevant Zn–Cr site under working conditions remains insufficiently resolved. Early descriptions of Zn–Cr catalysts often treated crystalline $ZnCr_2O_4$, defective spinel surfaces, or reduced $ZnCr_2O_x$ structures as relatively fixed catalytic surfaces. This approximation is useful for establishing elementary reaction pathways, but it becomes less reliable when the catalyst composition changes under a reducing syngas atmosphere. Theoretical studies have shown that partially reduced Zn–Cr surfaces can support different reaction routes toward methanol, ketene, and methane, and that the preferred pathway changes with adsorbate coverage and surface reduction state [8,9]. Operando investigations further indicate that Zn–Cr oxides undergo substantial structural evolution during CO hydrogenation, including progressive reduction, redistribution of Zn species, modification of local metal–oxygen coordination, and reconstruction of near-surface regions [10,11]. These observations suggest that the catalytically relevant surface may differ markedly from both the as-prepared oxide and the structure measured after reaction.

Oxygen vacancies are frequently considered key sites in this transformation because they modify the electronic structure of neighboring cations, strengthen CO adsorption, and facilitate C–O bond activation. Their catalytic role, however, cannot be described solely by vacancy concentration. The chemical properties of a vacancy depend strongly on the surrounding Zn, Cr, and O atoms, the oxidation state of nearby metal centers, and the presence of adsorbed hydrogen

or hydroxyl groups [12,13]. Vacancies located in different local coordination environments can therefore show substantially different adsorption energies and reaction barriers. Surface hydroxylation introduces an additional degree of complexity because hydrogen-rich syngas can stabilize hydroxylated configurations that are absent under vacuum or oxidizing conditions. Hydroxyl groups may participate directly in proton transfer, alter the stability of formyl, formate, methoxy, and ketene-related intermediates, and change the relative stability of reduced surface terminations. The active site should therefore be viewed as a local Zn–O–Cr structural motif whose composition and coordination respond continuously to the reaction environment rather than as an isolated oxygen vacancy embedded in an otherwise unchanged lattice. Comparable behavior has been reported for other Zn-containing mixed oxides. Studies on $ZnGaO_x$ and $ZnZrO_x$ indicate that oxygenate formation is governed by specific local metal–oxygen configurations rather than by bulk phase composition alone. Changes in cation arrangement, oxygen coordination, and surface reduction can alter the stability of methoxy-, formate-, and ketene-related intermediates and thereby redirect the subsequent reaction network [14,15]. Recent calculations of oxide–zeolite systems further suggest that methanol and ketene may originate from different oxide configurations and that the preferred oxygenate-forming site depends on the chemical potential of the surrounding reactants [16,17]. These findings are important because a change in the dominant oxygenate precursor can propagate through the entire bifunctional reaction network. A surface that favors methanol formation may interact differently with the zeolite than one that preferentially forms ketene or other reactive intermediates, ultimately affecting olefin, aromatic, and paraffin selectivity. Establishing the relationship between working-state oxide structure and oxygenate chemistry is therefore essential for understanding how oxide composition controls the overall performance of oxide–zeolite catalysts [18]. Characterizing such working-state structures remains challenging. Ex situ X-ray diffraction, X-ray photoelectron spectroscopy, electron microscopy, and related techniques mainly probe catalysts before or after reaction and can miss transient reduced, reconstructed, or hydroxylated configurations. Operando spectroscopy provides more direct information under reaction conditions, but experimentally observed signals often represent contributions from several coexisting species and local environments. Assigning a unique catalytic function to a specific Zn–Cr configuration is therefore difficult from spectroscopy alone. Conventional density functional theory calculations provide molecular-level information on adsorption structures and reaction barriers, but most studies examine only a small number of idealized surfaces with fixed stoichiometry. Variations in Zn/Cr ratio, oxygen chemical potential, hydrogen coverage, hydroxyl concentration, vacancy density, and surface reconstruction are frequently considered separately or neglected entirely. As a result, reaction pathways may be evaluated on surfaces that are energetically unfavorable under the actual temperature and gas composition used for syngas conversion. Such an approach can correctly describe the chemistry of a chosen model while still misidentifying the surface responsible for the measured catalytic behavior.

A more realistic description requires the thermodynamic stability of candidate surfaces to be evaluated before their catalytic activity is compared. In the present study, first-principles thermodynamics and density functional theory are combined to establish a working-state structural landscape for Zn–Cr–O catalysts under syngas conditions. More than 96 surface models are constructed by systematically varying the Zn/Cr ratio, oxygen chemical potential, hydroxyl coverage, degree of reduction, and oxygen-vacancy concentration. The relative stability of these structures is evaluated under H_2-rich reaction environments to identify surface configurations that are thermodynamically accessible during catalysis. Reaction pathways for CO activation and subsequent C–O hydrogenation are then calculated on the most relevant structures rather than on a single predetermined oxide termination. The resulting elementary-step energetics are incorporated into a microkinetic framework to connect the population of dynamically generated surface motifs with oxygenate formation rates and reaction selectivity. Particular attention is given to partially reduced Zn–O–Cr ensembles, where changes in local coordination can simultaneously modify CO adsorption, hydrogen transfer, vacancy stability, and C–O bond conversion. By linking surface thermodynamics, reaction kinetics, and active-site populations within a unified framework, this work aims to identify which Zn–Cr structures are actually present and catalytically relevant under working conditions. The resulting description provides a mechanistic basis for understanding why changes in composition, reduction degree, and reaction atmosphere alter oxygenate formation, and it offers a more transferable strategy for designing oxide components in bifunctional syngas-conversion catalysts. Rather than assigning activity to a fixed structural feature of the fresh material, the study establishes the active site as a reaction-induced structural ensemble whose abundance and reactivity are jointly determined by the surrounding chemical environment.

2. Materials and Methods

2.1. Surface Models and Reaction Conditions

A total of 96 Zn–Cr–O surface models were built to represent structures that may form during syngas conversion. The model set included stoichiometric Cr_2O_3, Zn-doped Cr_2O_3, $ZnCr_2O_4$, Zn-rich mixed oxides, oxygen-deficient surfaces, and hydroxyl-covered surfaces. The Zn/Cr atomic ratio ranged from 0 to 1.5. The surface oxygen-vacancy concentration ranged from 0 to 25%, while the hydroxyl coverage was set at 0, 0.25, 0.50, or 0.75 monolayers. The models were examined at 573–673 K and 1–5 MPa. H_2/CO ratios of 1, 2, and 3 were used to represent CO-rich, balanced, and H_2-rich feeds. These conditions cover the main range used for oxygenate production over Zn–Cr oxide catalysts.

2.2. Computational Design and Reference Models

The surface models were divided into four groups to examine the effects of Zn content, surface reduction, hydroxyl coverage, and gas composition. Stoichiometric Cr_2O_3 and $ZnCr_2O_4$ were used as reference surfaces. Zn-rich models were compared with these reference surfaces to

assess how local Zn–O–Cr structures affected CO adsorption and hydrogen transfer. Oxygen-deficient surfaces were included to represent the reduced states formed under H_2-rich conditions. Hydroxyl-covered surfaces were also considered because water and surface OH groups may form during C–O hydrogenation. Each reaction step was calculated on at least three surfaces with different local structures. This design reduced the risk of drawing conclusions from a single ideal model.

2.3. Density Functional Theory Calculations and Quality Control

Spin-polarized density functional theory calculations were performed using the projector-augmented-wave method and the PBE exchange–correlation functional. Dispersion forces were included by the D3 correction. The plane-wave cut-off energy was set at 450 eV, and the electronic convergence limit was 10^{-5} eV. All structures were relaxed until the force on each atom was below 0.03 eV Å^{-1}. Each slab contained at least four atomic layers and a 15 Å vacuum region. The bottom two layers were fixed, while the upper layers and adsorbed species were fully relaxed. The kkk-point mesh was checked by comparing $2\times2\times1$ and $3\times3\times1$ grids. Transition states were located with the climbing-image nudged elastic band method and confirmed by one imaginary frequency. The calculations were considered converged when the energy change remained below 0.03 eV after cut-off, slab-thickness, and kkk-point tests.

2.4. Surface Thermodynamics and Data Processing

The stability of each surface was assessed by atomistic thermodynamics. The surface free energy was calculated as

$$\gamma = \frac{G_{slab} - \sum_i N_i \mu_i}{2A},$$

where G_{slab} is the slab free energy, N_i is the number of atoms or adsorbed species of type i, μ_i is the related chemical potential, and A is the surface area. Temperature and pressure corrections for CO, H_2, H_2O, and O_2 were obtained from standard thermodynamic data. The predicted fraction of each surface was calculated from its relative free energy:

$$f_i = \frac{\exp(-\Delta G_i / k_B T)}{\sum_j \exp(-\Delta G_j / k_B T)},$$

where f_i is the fraction of surface i, ΔG_i is its free-energy difference from the most stable surface, k_B is the Boltzmann constant, and T is the temperature. Surfaces with predicted fractions below 1% were not included in the kinetic calculations.

2.5. Reaction Pathway and Microkinetic Analysis

The reaction network included CO adsorption, H_2 dissociation, and the stepwise formation of CHO*, CH_2O*, and CH_3O*. Methanol desorption and competing methane pathways were also considered. Adsorption energies and reaction barriers were calculated on the main surfaces selected from the thermodynamic analysis. Zero-point-energy and entropy corrections were added

to the reaction free energies. Rate constants were calculated by transition-state theory, and steady-state surface coverages were obtained by numerical integration. The predicted surface fractions were used as site-density inputs in the microkinetic model. This treatment avoided the assumption of one fixed active surface. Sensitivity analysis was used to identify the steps that controlled oxygenate formation. The effects of temperature, H_2/CO ratio, and reduced Zn–O–Cr site fraction were then examined. The model was tested with different initial coverages and time steps. A result was accepted when the change in the final oxygenate rate was below 1%.

3. Results and Discussion

3.1. Surface Stability under Syngas Conditions

The surface free-energy calculations indicated that the stable Zn–Cr–O structure varied with gas composition, temperature, and surface coverage. Stoichiometric Cr_2O_3 was stable under oxygen-rich conditions. Zn-containing and oxygen-deficient surfaces became more stable as the oxygen chemical potential decreased. Under H_2-rich syngas, partial oxygen removal formed low-coordinate Zn–O–Cr sites. Some reduced surfaces also retained hydroxyl groups because water was produced during CO hydrogenation. As shown in Fig. 1, no single surface structure remained stable across the full reaction range. Zn-rich surfaces were favoured at low oxygen chemical potentials, whereas surfaces with high hydroxyl coverage became less stable as the temperature increased. The fraction of reduced Zn–O–Cr sites rose with the H_2/CO ratio and exceeded 35% in the main oxygenate-forming region. This result indicates that the active surface develops during the reaction and differs from the fresh catalyst [19,20]. Pareras et al. (2025) also reported that Cr content and oxygen-vacancy concentration affect the structure and reduction behaviour of Cr-doped ZnO. Their calculations linked surface changes with CO adsorption and C–O bond cleavage. The current model also considers the Zn/Cr ratio, hydroxyl coverage, and gas chemical potential when selecting stable surface sites.

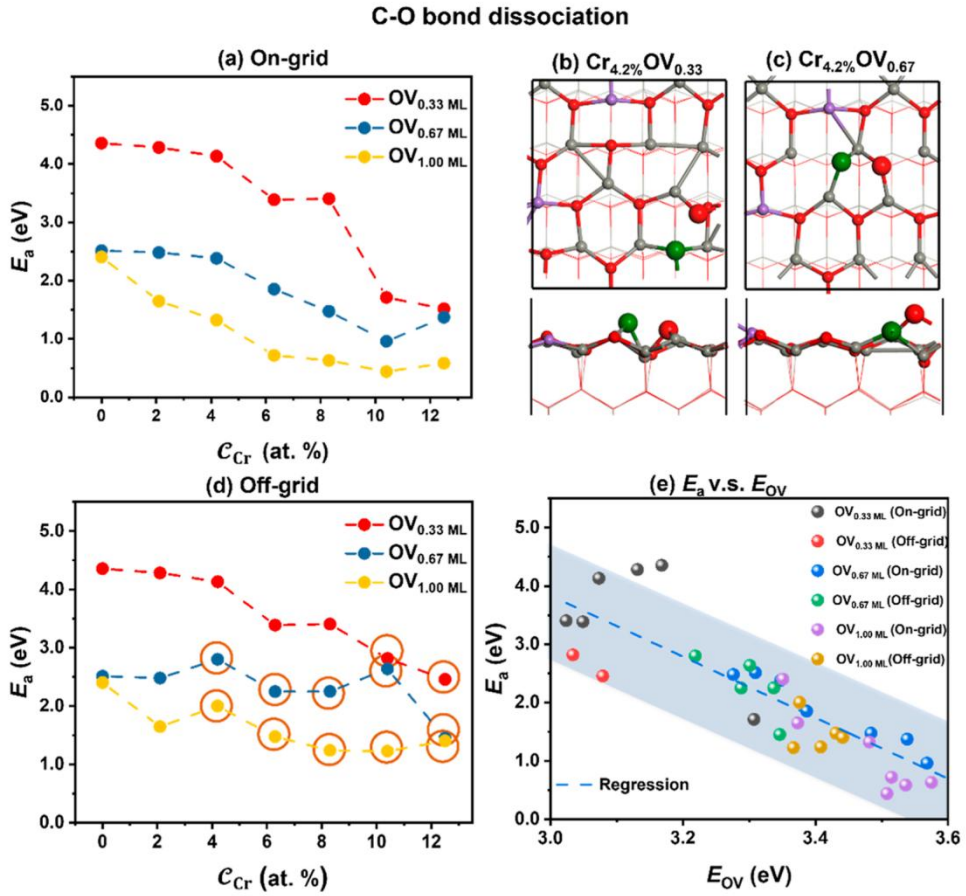

Fig. 1. Surface stability and reaction barriers of Zn–Cr–O models under different syngas conditions.

3.2. CO Activation and Stepwise Hydrogenation

The reaction barriers depended on the local arrangement of Zn, Cr, O, and oxygen vacancies. CO adsorbed weakly on stoichiometric Cr_2O_3, and its carbon atom remained far from the nearest surface hydrogen. The barrier for CH_3O* formation was therefore 1.21 eV. On the reduced mixed oxide, the CO-derived species adsorbed between a low-coordinate Zn atom and a nearby Cr–O site. Zn interacted with the oxygen end of the adsorbed species, while Cr and nearby hydroxyl groups assisted hydrogen transfer. As shown in Fig. 1, the barrier for CH_3O* formation decreased to 0.82 eV on the Zn-rich surface. Moderate reduction gave the lowest barrier because it created open adsorption sites without breaking the Zn–O–Cr structure. Strong reduction was less favourable. It weakened oxygenate adsorption and increased direct C–O bond cleavage, which could promote methane formation [21,22]. Stamatelos et al. (2026) reported a similar joint effect of Cr and oxygen vacancies on CO adsorption and C–O bond cleavage. Tiwari et al. (2026) also found that methanol, ketene, and methane pathways compete on reduced $ZnCr_2O_x$ surfaces. These results identify partly reduced Zn–O–Cr sites as the main structures for stepwise hydrogenation while limiting complete C–O bond cleavage.

3.3. Active-Site Fraction and Oxygenate Formation Rate

The microkinetic calculations indicated that the oxygenate formation rate depended on both site activity and site fraction. A site with a low reaction barrier made only a small contribution when its surface fraction was low. When reduced Zn–O–Cr sites accounted for less than 15% of the surface, the oxygenate rate remained close to that of stoichiometric Cr_2O_3. The rate increased rapidly as the fraction of reduced sites rose. As shown in Fig. 2, the oxygenate formation rate increased by 2.9 times when these sites accounted for more than 35% of the surface. This increase resulted from faster CO activation and lower barriers for CHO* and CH_2O* hydrogenation. Rate-control analysis identified early C–O hydrogenation as the main slow step on stoichiometric surfaces. Its effect decreased on Zn-rich reduced surfaces because the related barriers were lower. At stronger reduction levels, methanol desorption and the supply of adsorbed CO became more important. Wu et al. (2026) used microkinetic modelling to compare reactions on $ZnCrO_x$, SAPO-34, and their interface. They found that methanol formed on $ZnCrO_x$ could undergo carbonylation near zeolite acid sites and produce ketene. Their model used selected catalyst structures. By contrast, the current model weights each reaction rate according to the predicted fraction of the related oxide surface. This method links surface changes directly with oxygenate production.

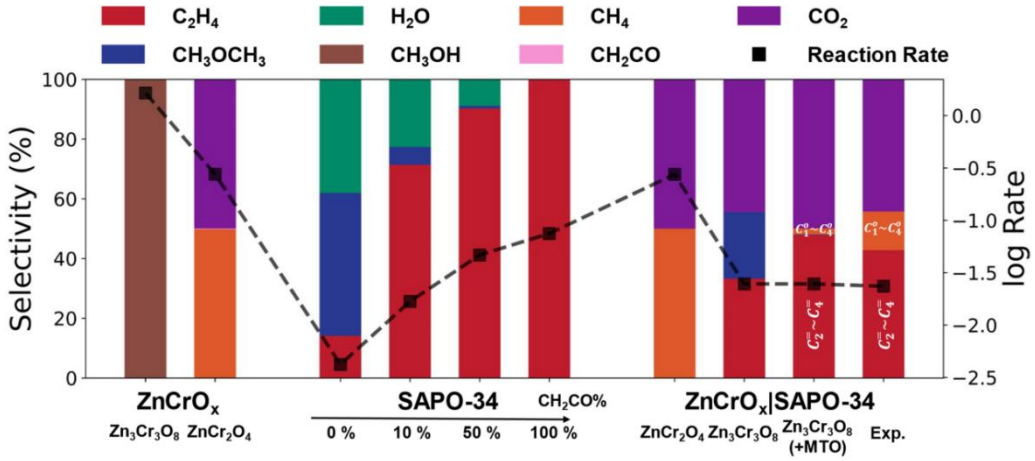

Fig. 2. Effect of reduced Zn–O–Cr sites on oxygenate formation and surface coverage.

3.4. Active-Site Formation during Reaction

The thermodynamic and kinetic results indicate that catalyst activity cannot be explained by Zn content or oxygen-vacancy concentration alone. Zn changed the local electronic structure, but the active geometry formed only after partial reduction under H_2-rich conditions. Oxygen removal exposed low-coordinate metal atoms, while the remaining bridging oxygen preserved the Zn–O–Cr structure needed for stepwise hydrogenation. Surface hydroxyl groups then supplied hydrogen to CO-derived species and promoted CH_3O* formation. This mechanism differs from models that assign activity to a fixed oxygen vacancy or a stoichiometric spinel surface. It also explains why ex situ measurements may fail to detect the working structure. Reduced sites may disappear when the catalyst is cooled or exposed to air. Recent screening studies found that dopants and oxygen

vacancies can lower CO activation barriers on many oxide surfaces [23,24]. However, these studies often rank sites only by reaction barriers and do not consider their fractions under working conditions. Both factors are required to explain the total reaction rate. The model still has several limits. It includes selected surface terminations, uses a mean-field treatment of adsorbate interactions, and does not contain a direct oxide–zeolite interface. Future work should examine larger reconstructed surfaces, coverage-dependent barriers, and operando measurements of Zn and Cr coordination. These tests may confirm how the fraction of reduced Zn–O–Cr sites changes with syngas composition.

4. Conclusion

The active sites of Zn–Cr–O catalysts changed with the reaction conditions. Surface thermodynamic calculations showed that partly reduced Zn–O–Cr sites were stable under H_2-rich syngas. These sites improved CO adsorption and hydrogen transfer. As a result, the barrier for CH_3O* formation decreased from 1.21 to 0.82 eV. The microkinetic model showed that the oxygenate formation rate increased by 2.9 times when reduced Zn–O–Cr sites covered more than 35% of the surface. These results link surface stability, active-site fraction, reaction barriers, and catalytic rate. They also show that catalyst performance depends on both site activity and the number of available sites. This method may help control the Zn/Cr ratio, reduction level, and syngas composition for oxygenate production. However, the model includes only selected surface structures and uses a mean-field treatment of adsorbed species. It also does not include direct contact between the oxide and zeolite. Further studies should use larger surface models, coverage-dependent barriers, and operando measurements to confirm the predicted Zn–O–Cr sites under reaction conditions.

References

1. Liang, S., Zhang, X., Du, Y., & Chen, W. (2026). Supply Network Restructuring and Capacity Ramp-Up Limits in the Localized Expansion of High-Performance Computing Equipment Production. Available at SSRN 7339738.

2. Yapeng, B. E. I., Xing, Y. U., Xianni, B. U., Yuhan, S. U. N., & Peng, G. A. O. (2025). Modified ZnZrOx coupled with ZSM-5 as the catalyst for the hydrogenation of CO2 to aromatics. Journal of Fuel Chemistry and Technology, 53(7), 1038-1049.

3. Yang, Z., Alexandrova, A. N., & Sautet, P. (2026). Modeling CO2 Hydrogenation to Methanol on an Ensemble of Inverse ZrO2 on Cu Catalytic Sites: Mechanism, Reactivity, and Deactivation. Angewandte Chemie, e5448247.

4. Belrhazi, I., Sair, S., Ait Ousaleh, H., Kongparakul, S., Samart, C., & Zahouily, M. (2026). Catalytic upgrading of HDPE into aromatic hydrocarbons via in situ and ex situ pyrolysis over metal-impregnated zeolite-based catalysts. Molecular Catalysis, 603, 116288.

5. Bao, Y., & Wang, H. (2026). Edge-to-Cloud Infrastructure Continuum: A Unified Framework for Optimizing Industrial IoT Systems. Available at SSRN 7185578.
6. Chen, F., Liang, H., Li, S., Yue, L., & Xu, P. (2025). Design of Domestic Chip Scheduling Architecture for Smart Grid Based on Edge Collaboration.
7. Kabwe, F. B., Jiang, Q., & Wang, C. (2026). Interfacial Active Sites in Catalysts for Higher Alcohol Synthesis From CO2: A Review. Chemistry–A European Journal, e71373.
8. Liang, R., Feifan, F. N. U., Liang, Y., & Ye, Z. (2025). Emotion-Aware Interface Adaptation in Mobile Applications Based on Color Psychology and Multimodal User State Recognition. Frontiers in Artificial Intelligence Research, 2(1), 51-57.
9. Pareras, G., & Rimola, A. (2025). Single-atom iron on silicon carbide surfaces as catalyst of Fischer-Tropsch-type reactions in astrophysical environments. Frontiers in Astronomy and Space Sciences, 12, 1605553.
10. Du, Y. (2025). Research on Digital Quality Traceability System for Temperature-Controlled Supply Chain of Foreign Trade Wine Driven by Blockchain and IoT. Business and Social Sciences Proceedings, 4, 57-65.
11. Stamatelos, I., Guo, Z., Pasel, J., & Saei, W. (2026). Oxide-derived metals and alloys: from dynamic reconstruction to function across electrocatalytic reactions. Energy Advances.
12. Tiwari, J. N., Bhaskaran, G., Kumar, K., Huh, Y. S., & Han, Y. K. (2026). Auto-Generated Valence States in Electrocatalysts for Boosting Oxygen and Hydrogen Evolution Kinetics in Alkaline Water/Alkaline Seawater/Simulated Seawater/Natural Seawater. Advanced Functional Materials, 36(45), e19158.
13. Jiao, Y., Zhao, B., Wang, A., & Shi, T. (2026). Construction and Empirical Study of a Modularized Teaching System for Art Courses Based on a Unified Training Pathway.
14. Yang, J. (2026). Stage-Coupled Computational Framework for Stratified Accessibility and Equity Analysis in Community-Based Elderly Care Services.
15. Bahou, S., Kosri, C., Ahmed, A. A., Mena, H., Sehrawat, R., Wohlrab, S., ... & Abdel-Mageed, A. (2026). Regulating Copper Nuclearity in Metal–Organic Frameworks for the Hydrogenation of Carbon Dioxide. Small Methods, e70882.
16. Wu, J., Wu, D., Zhang, J., & Peng, Y. (2026). Generative AI Feedback in Junior High School Artistic Creation Evaluation. Available at SSRN 7244838.
17. Bao, Y., Qiu, Y., & Wang, H. (2026, May). Unified Identity Layer for Hyperscale Ecosystems: A Framework for Cross-Platform User Attribution and Experimentation. In 2026 6th International Conference on Machine Learning and Intelligent Systems Engineering (MLISE) (pp. 540-543). IEEE.
18. Asif, M., Bilal, M., Hakeem, L., Asghar, G., Manzoor, S., Hira, ... & Khan, S. A. (2026). Catalytic Confinement Engineering for CO2 Conversion: From Catalytic Microenvironments to Sustainable Aviation Fuels. Carbon Neutralization, 5(4), e70186.

19. Gu, X. (2026). Identifying Causal Effects and Analyzing Heterogeneity of User Growth Interventions on Digital Platforms: Evidence from Large-Scale Behavioral Data. Available at SSRN 6809181.
20. Şahin, Ö., Ekinci, S., İzgi, M. S., & Onat, E. (2025). Effect of different solvents on hydrogen production from hydrolysis of potassium borohydride with a new and active Ni-based catalyst synthesized by green synthesis. International Journal of Hydrogen Energy, 143, 1098-1107.
21. Shown, B., Gogoi, P., Mitra, S., Shown, I., Bandyopadhyay, R., & Das, A. K. (2026). Emerging trends and future prospects of the catalytic conversion of syngas to higher alcohols. ACS Omega, 11(13), 19963-20001.
22. You, S. (2026). Verifiable Audit Mechanisms in AI Compliance Automation: Scalability. Available at SSRN 6547458.
23. Jiao, Y., Shi, T., Zhao, B., & Wang, A. (2026). The Impact of VR Sketching Simulations on the Assessment of Scale and Site Suitability in Public Art Spaces.
24. Lustemberg, P. G., Yang, C., Wang, Y., Ganduglia-Pirovano, M. V., & Woll, C. (2025). Synergistic effects in low-temperature CO oxidation on cerium oxide surfaces. Journal of the American Chemical Society, 147(8), 6958-6965.